

Towards Scalable Probabilistic Human Motion Prediction with Gaussian Processes for Safe Human-Robot Collaboration

Jinger Chong¹, Xiaotong Zhang¹, Kamal Youcef-Toumi¹

Abstract—Accurate human motion prediction with well-calibrated uncertainty is critical for safe human-robot collaboration (HRC), where robots must anticipate and react to human movements in real time. We propose a structured multitask variational Gaussian Process (GP) framework for full-body human motion prediction that captures temporal correlations and leverages joint-dimension-level factorization for scalability, while using a continuous 6D rotation representation to preserve kinematic consistency. Evaluated on Human3.6M (H3.6M), our model achieves up to 50 lower kernel density estimate negative log-likelihood (KDE NLL) than strong baselines, a mean continuous ranked probability score (CRPS) of 0.021 m, and deterministic mean angle error (MAE) that is 3–18% higher than competitive deep learning methods. Empirical coverage analysis shows that the fraction of ground-truth outcomes contained within predicted confidence intervals gradually decreases with horizon, remaining conservative for lower-confidence intervals and near-nominal for higher-confidence intervals, with only modest calibration drift at longer horizons. Despite its probabilistic formulation, our model requires only 0.24–0.35 M parameters, roughly eight times fewer than comparable approaches, and exhibits modest inference times, indicating suitability for real-time deployment. Extensive ablation studies further validated the choice of 6D rotation representation and Matérn 3/2 + Linear kernel, and guided the selection of the number of inducing points and latent dimensionality. These results demonstrate that scalable GP-based models can deliver competitive accuracy together with reliable and interpretable uncertainty estimates for downstream robotics tasks such as motion planning and collision avoidance.

I. INTRODUCTION

Human motion prediction plays a crucial role in applications such as autonomous driving, sports analysis, and human-robot collaboration (HRC). As robots increasingly operate in shared environments with humans, accurately anticipating human motion has become essential for safe, efficient, and seamless interactions. In tasks such as collaborative assembly or assistive care, predicting human movements enables robots to plan ahead, make informed decisions, and avoid potential collisions. The stochastic and multimodal nature of human motion presents a fundamental challenge, making uncertainty quantification as critical as prediction accuracy itself. Reliable uncertainty estimates allow systems to evaluate confidence in their predictions, supporting adaptive decision-making in dynamic and safety-critical environ-

ments [1], [2]. Despite substantial progress, most current methods either prioritize accuracy without interpretability or require substantial computational resources, limiting their practicality in real-time HRC scenarios.

Probabilistic approaches address this challenge by predicting human motion as distributions rather than deterministic outcomes. Recent state-of-the-art (SOTA) probabilistic methods leverage deep learning architectures, including graph-based networks [3], transformers [4], and diffusion models [5], to capture complex, multimodal motion patterns. While these methods demonstrate strong predictive performance, they face critical limitations for HRC. Many deep learning models act as “black boxes,” offering little insight into their decision-making process, which is problematic in safety-sensitive applications. Moreover, the computational cost and inference latency of these architectures can impede deployment in real-time systems [6], creating a practical gap between research performance and actionable HRC applications.

In contrast to deep learning approaches, Gaussian Processes (GPs) offer a complementary probabilistic framework that provides inherent uncertainty estimates and interpretable predictions. However, conventional GP-based motion prediction methods have historically been limited in scalability, restricting their application to low-dimensional or partial-body motion data [7]. For example, the approach in [7] models constrained probabilistic motion prediction for human arms, focusing on only three joints per arm, corresponding to six joint angles in total. The method employs an autoregressive formulation with a separate GP trained for each joint angle and performs multi-step predictions through iterative rollouts. In addition, predicted joint distributions are transformed from joint space to task space using Jacobian-based mappings and modified through Monte Carlo rejection sampling to enforce kinematic and workspace constraints. While this design enables physically consistent predictions, the combination of sequential rollouts, Jacobian transformations, and sampling-based constraint enforcement introduces additional computational overhead that becomes increasingly expensive as the number of joints and prediction steps increases. As a result, the framework is demonstrated only on arm trajectories and evaluated on relatively small datasets, leaving its applicability to full-body motion modeling unclear.

Building on this work, we develop a scalable GP-based framework capable of modeling full-body human motion on a large-scale dataset. Our approach integrates multitask [8] and variational [9] GP techniques, employs factorized out-

*This research was made possible by the support and partnership of King Abdulaziz City for Science and Technology (KACST) through the Center for Complex Engineering Systems at Massachusetts Institute of Technology (MIT) and KACST.

¹Department of Mechanical Engineering, Massachusetts Institute of Technology, Cambridge, MA 02139, USA. jinger@mit.edu, kevxt@mit.edu, youcef@mit.edu

puts for computational efficiency, and predicts future motion in a one-shot manner that explicitly captures temporal correlations across the prediction horizon. In addition, we use a continuous 6D rotation representation, which aligns better with GP assumptions and avoids the discontinuities and representation ambiguities present in common rotation representations such as Euler angles and quaternions. This design balances model expressivity, interpretability, and computational feasibility, positioning GPs as a practical alternative for probabilistic motion prediction in HRC.

In this work, we make the following contributions: (i) we pioneer the extension of GPs to full-body human motion modeling on large-scale datasets such as Human3.6M (H3.6M) [10], overcoming the limitations of prior partial-body approaches; (ii) we demonstrate that a continuous 6D rotation representation significantly improves alignment with GP assumptions, enhancing predictive fidelity; (iii) we design a multitask variational GP architecture that achieves interpretable uncertainty estimates and computational efficiency, making it practical for real-time HRC applications; (iv) we achieve superior probabilistic performance with fewer parameters than existing deep learning baselines; and (v) we release a public preprocessing pipeline that reconstructs the legacy exponential map archive of H3.6M data [11] and includes verification and 3D visualization tools, enabling reproducible and transparent research.

Collectively, our work positions GPs not only as a competitive alternative to modern deep learning approaches but also as an interpretable and practically deployable solution for probabilistic human motion prediction in real-world HRC applications.

II. RELATED WORK

A. Probabilistic Human Motion Prediction

Human motion prediction methods can be broadly categorized as deterministic, stochastic, or probabilistic. Deterministic approaches predict a single future trajectory and often fail to capture the inherent variability of human motion over longer horizons [12]. To address this, stochastic methods generate multiple potential futures [4], [13], [14], [12]. However, these methods often prioritize diversity over plausibility, limiting their applicability in robotics tasks that require both accuracy and reliability [3], [5].

Probabilistic approaches provide a principled way to explicitly model uncertainty through probability distributions over future trajectories. This enables both estimation of multiple potential outcomes and the integration of confidence measures into downstream tasks such as motion planning, improving safety and execution time in HRC [1], [2], [15]. Existing probabilistic strategies include Bayesian networks [15], graph-based networks [3], diffusion models [5], invertible networks [6], and GPs [16]. While many of these approaches are highly expressive, they can require larger datasets, complex architectures, or longer inference times, which may complicate their deployment in real-time HRC applications. For these reasons, we adopt GPs in our framework.

B. Gaussian Processes for Dynamical Systems

Gaussian processes (GPs) have been widely used to model dynamical systems due to their ability to capture nonlinear relationships. However, conventional GPs scale poorly with high-dimensional inputs and outputs, which has limited their application in human motion prediction. For example, prior work has focused on partial-body motion such as arm trajectories involving only a small set of joints [7].

To address scalability, several approaches learn lower-dimensional latent representations, as in GP-LVMs [16], [17]. While effective for reducing dimensionality, latent representations obscure the original joint space and make uncertainty estimates less interpretable. In contrast, our framework maintains the original joint representation and instead factorizes the GP at the joint–dimension level, enabling tractable computation for full-body motion. Conventional GP approaches also often treat outputs as independent, overlooking dependencies that have been shown to improve performance across applications, including leg and upper-body motion capture forecasting [18]. We address this by incorporating multitask GP extensions [8] to capture temporal correlations across the prediction horizon.

Another limitation of standard GP models is their cubic complexity with respect to the number of observations, which restricts their use to relatively small datasets. To overcome this, we employ sparse variational approximations with inducing points [9], enabling efficient training on a large-scale human motion dataset. Together, these design choices allow scalable, interpretable, and temporally coherent full-body motion prediction with GPs.

C. Pose Representations for Human Motion Prediction

Human poses can be represented in multiple ways, each with trade-offs. Position-based representations, such as 3D joint coordinates [13], [19], [20], are straightforward to optimize but may violate bone-length constraints, producing physically implausible poses.

Rotation-based representations in $SO(3)$, including Euler angles [7], exponential maps [6], [11], and quaternions [3], [21], preserve kinematic consistency but introduce challenges for regression. Euler angles are discontinuous, quaternions lie on a manifold, and Euclidean distances in these spaces may poorly reflect actual rotational differences. These limitations have motivated our use of smooth, continuous embeddings for rotation regression in human motion prediction.

D. Model Efficiency in Human Motion Prediction

Human motion prediction models vary widely in size and computational cost. Deterministic approaches tend to be compact, with simple architectures such as SiMLPe which uses a single MLP with DCT preprocessing having around 0.1–0.2 M parameters [19]. Slightly larger deterministic models, like HisRepItself [19], use roughly 3–4 M parameters.

Stochastic methods are generally heavier, often ranging from 7 M to over 30 M parameters [13], [20], [22], due to more complex architectures and sampling procedures.

Probabilistic methods [3], [6] are typically similar in scale to deterministic methods, roughly 0.3–2 M parameters, though sequential or autoregressive rollouts can introduce additional computational overhead.

While parameter count is not directly equivalent to training or inference speed, it provides a rough indication of computational efficiency. In this context, GP models often require additional computation for kernel evaluations and inversions, but small, sparse, or factorized GP architectures can be efficiently parallelized. This enables competitive runtime and opens the door for online learning and real-time deployment.

III. PROBLEM FORMULATION

The goal of this work is to predict probability distributions over human joint poses $s_i \in \mathbb{R}^{J \times D}$, where J denotes the number of joints defining the human skeleton and D specifies the dimensionality of the chosen pose representation for each joint. At time step t , given past observations $\mathbf{x}_t = \{s_{t-H+1}, \dots, s_t\}$, with H as the observation window, we aim to estimate the distributions of future poses $\mathbf{y}_t = \{s_{t+1}, \dots, s_{t+F}\}$ over a prediction horizon of F time steps. Formally, this can be expressed as $p(\mathbf{y}_t | \mathbf{x}_t)$. Depending on the experimental setup and evaluation metric, the input and output pose representations, along with their dimensionalities, may vary.

IV. METHODOLOGY

A. Architecture Overview

Human motion prediction is often formulated in two ways: autoregressive rollout [6], [7] or one-shot forecasting [3].

In the autoregressive setting, future poses are generated sequentially

$$p(\mathbf{y}_t | \mathbf{x}_t) = \prod_{f=1}^F p(s_{t+f} | \mathbf{x}_t, s_{t+1:t+f-1}) \quad (1)$$

where each predicted step depends on all previously predicted steps. While this explicitly models temporal dependencies, uncertainty accumulates recursively, often producing over-dispersed predictions at longer horizons.

In contrast, one-shot forecasting predicts all future steps jointly

$$p(\mathbf{y}_t | \mathbf{x}_t) = p(s_{t+1:t+F} | \mathbf{x}_t), \quad (2)$$

yielding a single joint distribution over the prediction horizon. We adopt this approach to avoid compounding uncertainty and directly capture correlations across future steps.

A naive GP formulation for one-shot full-body human motion prediction maps $\mathbb{R}^{H \times J \times D} \rightarrow \mathbb{R}^{F \times J \times D}$, which for typical values ($J = 20$, $D = 6$, $F = 50$) results in 6000 output dimensions, making training computationally infeasible. To address this, we factorize the problem across joint–dimension pairs, modeling each pair with a separate GP as shown in Fig. 1.

$$f_{j,d} : \mathbb{R}^H \rightarrow \mathbb{R}^F \quad (3)$$

Each GP takes the past trajectory of length H as input and produces a Gaussian predictive distribution over F

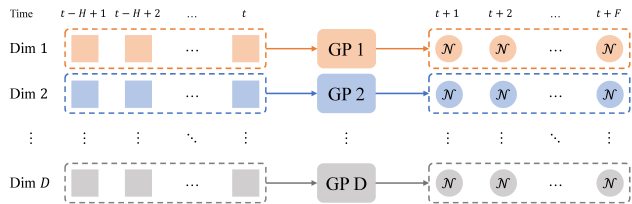


Fig. 1. Model architecture illustrated for a single joint with D dimensions. Each joint–dimension pair is modeled by a GP that maps H past time steps to F future time steps and produces a Gaussian predictive distribution at each future time step. This structure is replicated for all joints, resulting in 96 parallel GPs after preprocessing.

future steps. After removing zero-variance dimensions during preprocessing, this results in 96 independent GPs. Each GP captures temporal correlations within its prediction horizon, while cross-joint and cross-dimension dependencies are not modeled explicitly.

This approximation is reasonable in the short-horizon setting, where motion evolves smoothly and future behavior is largely determined by recent temporal history. At these time scales, short-term dynamics dominate, and modeling per-dimension temporal structure captures most of the predictive signal. The resulting factorization enables scalable training without sacrificing short-term predictive accuracy.

B. GP Formulation

Building on the one-shot prediction framework, each GP is multitask, jointly predicting multiple output dimensions. To capture temporal correlations across these outputs, the GPs are dependent via a linear model of coregionalization (LMC) with L latent functions.

To scale to large datasets, we adopt sparse variational approximation [9], introducing M inducing variables. This reduces the computational complexity from $O(N^3)$ to $O(NM^2)$ per GP, where N is the number of training samples.

Each GP produces an analytical Gaussian distribution over its F future steps,

$$\mathbf{y}_{j,d} \sim \mathcal{N}(\boldsymbol{\mu}_{j,d}, \boldsymbol{\Sigma}_{j,d}), \quad (4)$$

as illustrated in Fig. 1. This provides well-calibrated uncertainty estimates. For consistency with evaluation metrics in prior work, we also draw Monte Carlo samples from these distributions.

Finally, input similarity is encoded using a Matérn 3/2 kernel with an additive linear term

$$k(\mathbf{x}, \mathbf{x}') = \sigma^2 \left(1 + \frac{\sqrt{3}r}{\ell} \right) \exp \left(-\frac{\sqrt{3}r}{\ell} \right) + \sigma_{\text{lin}}^2 \mathbf{x}^\top \mathbf{x}' \quad (5)$$

where $r = \|\mathbf{x} - \mathbf{x}'\|$, ℓ is the length scale, σ^2 the Matérn variance, and σ_{lin}^2 scales the linear contribution. The Matérn term captures local smoothness, while the linear term accounts for long-term drift.

C. Pose Representation

Human poses can be parameterized either as 3D joint positions or as joint rotations. Position-based representations are straightforward to optimize but do not inherently enforce kinematic constraints. Since valid poses lie on a nonlinear manifold defined by fixed bone lengths, direct regression in position space can produce physically implausible configurations, and Euclidean kernels may poorly reflect actual pose differences. This can lead to both inaccurate predictions and miscalibrated uncertainty estimates.

Rotation-based representations preserve bone-length consistency when combined with forward kinematics (FK). Common parameterizations, however, often introduce discontinuities or manifold constraints, making Euclidean distances in parameter space a poor proxy for rotational differences. These issues violate the smoothness assumptions of our kernel.

To address these limitations, we adopt a 6D rotation representation [23]. Each rotation matrix is represented by stacking its first two columns into a 6D vector, which is mapped back to a valid rotation via differentiable Gram–Schmidt orthonormalization. This defines a smooth, continuous embedding where Euclidean distances meaningfully approximate local rotational differences. Combined with FK, this approach preserves bone-length consistency and enables stable GP regression. Ablation studies confirm that this representation outperforms alternatives in probabilistic metrics, justifying its use in our model.

V. EXPERIMENTS

A. Dataset

We evaluated our approach on the H3.6M dataset [10], a widely used benchmark for human motion prediction. H3.6M contains motion capture data from 11 subjects performing 15 everyday activities, recorded at 50 Hz with a Vicon system. The dataset provides 3D joint angles for 25 body joints, represented as intrinsic ZXY Euler angles in degrees relative to their parent joints, along with the global XYZ translation of the root joint. Following prior work [3], [6], and to reduce data redundancy, all sequences were downsampled by a factor of two, yielding an effective frame rate of 25 Hz.

For probabilistic and stochastic evaluations, subjects S9 and S11 were reserved as test subjects, subsampled to every 25th frame, whereas for deterministic evaluation, only subject S5 was used, selecting 256 random frames per action. To monitor training progress, a small validation set was constructed by selecting every 100th frame from the same test subjects. While this follows the standard benchmark protocol [3] and allows comparability with prior work, we note that in practical applications, using frames from test subjects for validation could introduce a minor form of information leak. The validation frames are sparsely sampled to provide a rough estimate of model performance during training without overly biasing results.

B. Implementation

We first removed the global root translation, which is known to be corrupted [3], as well as static joints exhibiting zero variance across the dataset, leaving 20 joints. We then converted joint angles to the desired pose representation.

To promote reproducibility and facilitate future research, we provide a public repository¹ containing scripts that replicate the full preprocessing pipeline, along with utilities for FK, 3D skeleton visualization, and metric computation. Several prior works [6], [3] reference a now-unavailable ZIP archive [11] containing preprocessed H3.6M data in exponential map format. Our repository can recreate this from the official raw H3.6M data and includes a verification script to ensure numerical consistency with the legacy archive.

We generated training pairs using sliding windows of sizes H and F . Dimensions with zero variance were then removed. Unlike the initial filtering step, which eliminated entire static joints, this step prunes individual joint dimensions that do not vary (e.g., Y Euler angle of the elbow), while retaining other active dimensions of the same joint. The remaining data was normalized across joint dimensions and time steps to zero mean and unit variance, and the statistics were saved for use during evaluation. Finally, the dataset was structured so that each joint dimension constitutes an independent time series mapping past H steps to future F steps.

Following Motron [3], we set H and F according to the values in Table I. Inducing points were initialized from mini-batch K-means cluster centers using `SciPy` and GP models were implemented with `GPYtorch`. Training was parallelized via a `ModelList`, and the total evidence lower bound (ELBO) was optimized using natural gradient descent (NGD) for variational parameters and Adam for hyperparameters. Additionally, cosine learning rate decay was applied to Adam after a warmup period, and early stopping was employed. Table I summarizes the selected model and training settings. Our code and trained weights are also released publicly².

C. Metrics

We evaluated our model using metrics that enabled direct comparison with prior work [3], [6], organized into four categories: probabilistic, deterministic, stochastic, and model efficiency.

Probabilistic. We generated 1000 samples of predicted rotations and converted them to 3D joint positions via FK, ignoring certain joints following Motron [3]. Kernel density estimate negative log-likelihood (KDE NLL) was calculated per batch of size 20 and per joint, with NLL summed across joints and clipped to a maximum of 20. Using the first 50 samples, we also reported the continuous ranked probability score (CRPS) and evaluated empirical coverage at 50%, 80%, and 95% confidence levels by computing the fraction of ground-truth positions within the predicted intervals.

¹<https://github.com/jingerchong/h36m-tools>

²Link will be included in the final version.

TABLE I

GP IMPLEMENTATION PARAMETERS FOR PROBABILISTIC/STOCHASTIC AND DETERMINISTIC EVALUATIONS. INPUT AND OUTPUT HORIZONS ARE REPORTED AS NUMBER OF FRAMES, WITH THE EQUIVALENT DURATION IN SECONDS IN PARENTHESES.

Parameter	Probabilistic/Stochastic	Deterministic
Input H	12 (0.5 s)	50 (2 s)
Output F	50 (2 s)	25 (1 s)
Inducing M	25	25
Latent L	3	3
<hr/>		
K-means batch	4096	
Train batch	2048	
Val batch	512	
<hr/>		
NGD LR	0.4	0.45
Adam LR max	0.04	0.075
Warmup	3	
Early stop	10	
Min delta	0.005	
Max epochs	50	
<hr/>		
Seeds	0, 1, 2	
GPU	RTX 3070 Ti	

Deterministic. To quantify rotational accuracy, the predicted rotation was computed as the mean rotation in $SO(3)$ over 50 samples. This mean rotation was then converted to intrinsic ZYX Euler angles in radians, and the L2 norm of the error was obtained over the flattened vector spanning all joints and dimensions. Averaging in $SO(3)$ ensures that the mean rotation respects the geometry of the rotation manifold rather than simply averaging Euler angles in Euclidean space.

Stochastic. We reported best-of-50 average displacement error (ADE) and final displacement error (FDE), as well as average pairwise distance (APD) computed over all 50 samples, in the same 3D joint space as the probabilistic evaluation with the same joints ignored. These metrics are intended solely for benchmarking, as the model was not explicitly optimized for trajectory-level accuracy or diversity.

Model Efficiency. We counted the number of learnable parameters as a measure of model complexity and memory footprint. Although parameter count does not directly determine runtime, it provides a useful proxy for model comparison. Additionally, we measured the average inference time of our model over 1000 forward passes to indicate real-time suitability.

D. Ablation Studies

Extensive ablation studies were conducted to evaluate the impact of various design choices and hyperparameters on predictive performance. Specifically, we compared different pose representations, covariance kernels, numbers of inducing points M , numbers of latent dimensions L , and batch sizes, with learning rates tuned appropriately for each setting. Table II summarizes the range of settings explored for each factor, which we combined to identify the configuration that achieves the best overall accuracy and uncertainty calibration while remaining lightweight.

TABLE II

SETTINGS EVALUATED IN ABLATION STUDIES

Factor	Options Tested
Pose representation	exponential map, quaternion, 6D rotations
Covariance kernel	RBF, Matérn 3/2, Matérn 5/2 (+ Linear)
Inducing M	10, 25, 50, 100, 200
Latent L	1, 2, 3, 4, 6
Batch size	256, 512, 1024, 2048, 4096

VI. RESULTS

A. Pose Representations

Fig. 2 presents the first ablation study, evaluating the impact of different rotation representations on our metrics. Using the 6D rotation representation resulted in a noticeable improvement in KDE NLL, whereas the exponential map and quaternion representations exhibited similar performance. Based on these results, all subsequent ablation studies were conducted using the 6D rotation representation, as it consistently provided the best probabilistic performance.

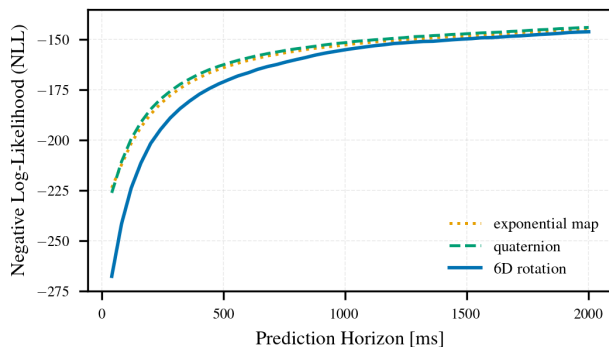


Fig. 2. KDE NLL for different rotation representations evaluated in our ablation study. Exponential map and quaternion representations show similar performance, while 6D rotation consistently achieves the lowest KDE NLL, most evidently at shorter horizons.

B. Probabilistic Evaluation

As shown in Fig. 3, our method achieves consistently lower KDE NLL than DLow [13] and Motron [3]. At early time steps, DLow exhibits high positive NLL values, reflecting overconfident but inaccurate predictions, whereas our model maintains low negative values, indicating accurate and confident probabilistic predictions. Across the full 2 s horizon, our model achieves a total NLL advantage of 20–50 over Motron, corresponding to an average per-joint improvement of 1–3, which translates to the ground-truth pose receiving 3–20 \times higher probability density compared to Motron.

In practical terms, by assigning higher likelihood to the true human motion, our model enables a robot operating alongside a human to anticipate actions, coordinate movements effectively, and plan responsive behaviors. This advantage is particularly pronounced at short horizons, where

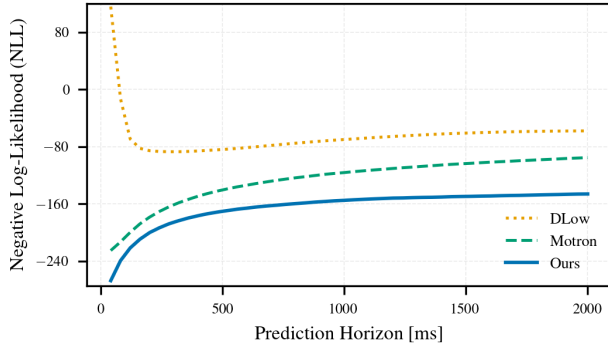


Fig. 3. KDE NLL of our final model compared to Motron and DLow. Our model consistently achieves lower KDE NLL across all time steps, indicating stronger probabilistic performance.

timely predictions are essential for fluid collaboration and assistance.

We further assessed probabilistic calibration using CRPS. Our model achieved a mean CRPS of 0.021 m, with per-frame values ranging from 0.002 m in early frames to 0.030 m in later frames. The CRPS quantifies the discrepancy between the predicted cumulative distribution and the ground-truth joint positions, capturing both bias and spread of the predictions. Lower CRPS indicates that the predicted distributions are well-centered around the true motion and have appropriate variance, corresponding to deviations of only a few centimeters per joint, and ensuring that sampled trajectories realistically reflect the stochasticity of human motion without being over- or under-confident.

Coverage analysis in position space, shown in Fig. 4, indicates that empirical coverage gradually decreases with increasing prediction horizon. At short horizons, the 50% interval is strongly conservative, containing more actual outcomes than expected. Coverage for the 50% and 80% intervals decreases with horizon but remains above nominal, while the 95% interval stays close to nominal throughout. This conservatism enhances safety by accounting for a wider range of possible human motions, reducing collision risk, while the well-calibrated 95% interval ensures reliable high-confidence predictions. Overall, calibration is stable across time with only modest drift at longer horizons. Combined with the KDE NLL and CRPS results, these findings show that the model produces accurate and practically well-calibrated uncertainty estimates suitable for dynamic and safety-critical HRC.

To illustrate the predicted uncertainty distributions, Fig. 5 shows sampled skeleton predictions from the model at different prediction horizons. The increasing dispersion of the samples reflects the model’s growing uncertainty in future motion as the horizon extends. An accompanying video³ demonstrates these predictions for example motion sequences and across multiple action types.

³<https://youtu.be/vxXdQkI0o30>

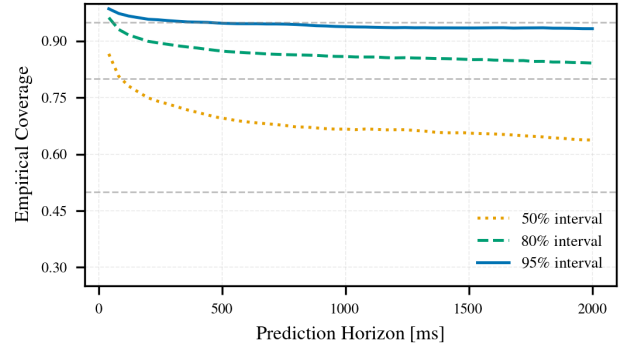


Fig. 4. Empirical coverage of predicted joint positions at 50%, 80%, and 95% confidence intervals across prediction horizons. The 50% interval is highly conservative at short horizons and gradually decreases while remaining above nominal at longer horizons. The 80% interval shows slight overestimation early on and stabilizes over time, while the 95% interval remains close to nominal throughout. Overall, the model exhibits modest calibration drift with horizon, maintaining reliable uncertainty estimates.

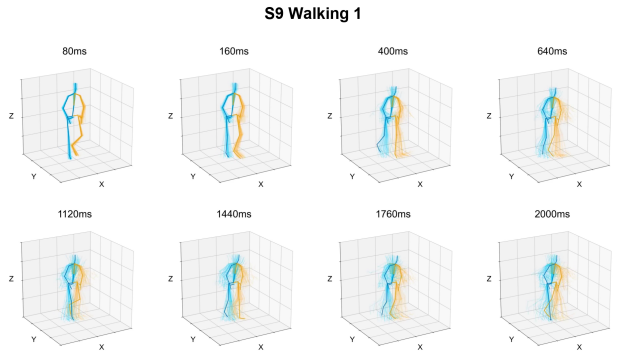


Fig. 5. Visualization of 50 sampled skeleton predictions drawn from the predicted distributions at different horizons. The solid skeleton denotes the ground-truth motion, while the translucent skeletons represent sampled predictions. Example shown for Subject S9 performing the walking action (first sequence). Colors indicate body sides (blue: right, orange: left) for visual clarity. The increasing spread of samples at longer horizons reflects the growth of predictive uncertainty over time.

C. Deterministic Evaluation

Table III reports the deterministic performance of our model in terms of MAE, computed on the mean rotations of the distribution, reflecting the central tendency of the predicted motions. Across the full 1 s prediction horizon, our method remains competitive, with MAE differences relative to the strongest baseline ranging from approximately 3% to 18%. As discussed in the previous subsection, the predicted distributions are conservative at short horizons, producing wider spreads that can shift the mean away from ground truth thereby slightly increasing MAE. At longer horizons, coverage gradually approaches nominal levels, making the mean predictions more representative and narrowing the performance gap to Motron. These results show that our model maintains reasonable deterministic accuracy even while primarily optimizing for probabilistic predictions.

Fig. 6 highlights the evolution of the mean predicted poses over different horizons. Consistent with the increasing MAE

TABLE III

MAE OF OUR MODEL COMPARED TO SOTA. IMPROVEMENT AT LONGER HORIZONS COULD BE DUE TO MEAN PREDICTIONS BECOMING MORE REPRESENTATIVE AS COVERAGE APPROACHES NOMINAL LEVELS. GRU SUP AND QUARTERNET RESULTS ARE ONLY REPORTED UP TO 400 MS AS LONGER-HORIZON EVALUATIONS WERE NOT PROVIDED IN THE ORIGINAL WORKS.

ms	80	160	320	400	560	720	880	1000
Zero Vel [3]	0.40	0.70	1.11	1.25	1.46	1.63	1.76	1.84
GRU sup [11]	0.43	0.74	1.15	1.30	-	-	-	-
Quarternet [21]	0.37	0.62	1.00	1.14	-	-	-	-
HisRepItself [24]	0.28	0.52	0.88	1.02	1.23	1.40	1.55	1.64
Motron [3]	0.28	0.51	0.87	1.01	1.22	1.40	1.54	1.63
Ours	0.33	0.62	1.02	1.16	1.36	1.50	1.61	1.68

reported in Table III, the predictions gradually deviate from the ground-truth motion at longer horizons, illustrating the challenge of accurate long-term forecasting. An accompanying video⁴ demonstrates these predictions over short motion sequences and across action types.

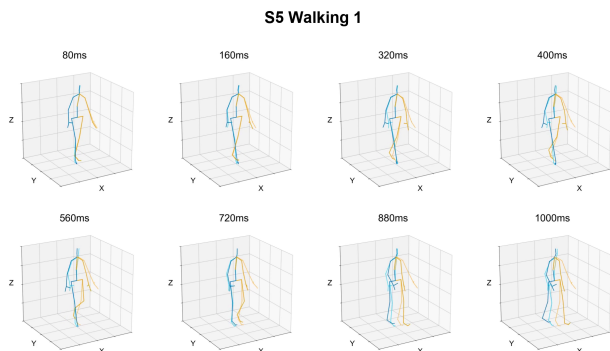


Fig. 6. Visualization of mean skeleton predictions at different horizons. The solid skeleton denotes the ground-truth motion, while the translucent skeleton represents the mean prediction. Example shown for Subject S5 performing the walking action (first sequence). Colors indicate body sides (blue: right, orange: left) for visual clarity. As horizon increases, the deviation from the ground-truth motion becomes more pronounced.

D. Stochastic Evaluation

Table IV presents trajectory-level metrics ADE, FDE, and APD, computed over 50 sampled trajectories. Each trajectory is generated by independently sampling each joint-dimension GP at every timestep, so the resulting sequences of full human poses may lack temporal consistency across frames. Because each sample is not temporally coherent, best-of-50 metrics such as ADE and FDE are artificially inflated, and APD is reduced, relative to stochastic baselines that model entire trajectories jointly. These metrics serve as secondary reference measures, while the main strength of our model lies in accurately representing probabilistic distributions over possible future motions.

⁴<https://youtu.be/vxXdQkI0o30>

TABLE IV

APD, ADE, AND FDE OF OUR MODEL COMPARED TO SOTA. SLIGHTLY HIGHER ADE/FDE AND LOWER APD ARE EXPECTED, AS OUR MODEL FOCUSES ON PROBABILISTIC DISTRIBUTIONS RATHER THAN SINGLE-SAMPLE TRAJECTORIES.

	1 s			2 s		
	APD \uparrow	ADE \downarrow	FDE \downarrow	APD \uparrow	ADE \downarrow	FDE \downarrow
DSF [25]	-	-	-	9.330	0.493	0.592
MT-VAE [26]	-	-	-	0.403	0.457	0.595
MotionDiff [22]	-	-	-	15.353	0.411	0.509
HumanMAC [20]	-	-	-	6.301	0.369	0.480
ProbHMI [6]	-	-	-	6.682	0.364	0.493
DLow [13]	5.180	0.305	0.419	11.741	0.425	0.518
Motron [3]	3.453	0.252	0.350	7.168	0.375	0.488
Ours	3.166	0.400	0.447	5.722	0.545	0.542

E. Model Efficiency

Table V summarizes the number of parameters of our model compared to several SOTA methods in human motion prediction. Our probabilistic/stochastic variant employs only 0.24M parameters, while the deterministic variant uses 0.35M. The difference is due to variations in input-output dimensionality under the evaluation setup. Both variants are as compact as SiMLPe [19], which uses a deterministic DCT+MLP architecture, and ProbHMI [6], which implements an autoregressive GCN/RNN model. Remarkably, our approach requires roughly $8\times$ fewer parameters than Motron [3] while achieving superior NLL performance and comparable deterministic accuracy, making it the most parameter-efficient choice among probabilistic and stochastic models when uncertainty modeling is desired.

TABLE V

NUMBER OF PARAMETERS FOR VARIOUS SOTA METHODS. OUR MODEL USES THE FEWEST PARAMETERS AMONG PROBABILISTIC AND STOCHASTIC APPROACHES WHILE ACHIEVING THE STRONGEST PROBABILISTIC PERFORMANCE (KDE NLL).

	Type	Method	Params
SiMLPe [19]	Deterministic	DCT, MLP	0.14M
HisRepItself [24]	Deterministic	Attention, GCN	3.24M
DLow [13]	Stochastic	Latent, CVAE	7.30M
MotionDiff [22]	Stochastic	Diffusion	29.93M
HumanMAC [20]	Stochastic	DCT, Diffusion	28.40M
Motron [3]	Probabilistic	Latent, GNN	1.67M
ProbHMI [6]	Probabilistic	GCN and RNN	0.31M
Ours	Probabilistic/Stochastic	GP	0.24M
	Deterministic	GP	0.35M

In terms of inference speed, our current probabilistic implementation processes sequences in approximately 560–685 ms. This latency is largely attributable to the sequential evaluation of 96 GPs, constrained by the current parallelism limitations of GPyTorch. On average, this corresponds to 6–7 ms per GP per sequence, indicating substantial room for acceleration through parallel computation. Therefore, our framework is inherently suitable for real-time deployment, and the observed computational overhead is an implement-

tation artifact rather than a fundamental limitation of the proposed model.

VII. CONCLUSION

This work demonstrates the potential of GPs for accurate full-body human motion prediction through a structured multitask variational GP framework that leverages a 6D rotation representation and joint-dimension-level factorization for scalability. Our model achieves up to 50 lower KDE NLL, a mean CRPS of 0.021 m, and competitive deterministic accuracy 3–18% higher than SOTA baselines, while using only 0.24–0.35 M parameters, roughly eight times fewer than comparable probabilistic models, highlighting its efficiency in capturing uncertainty with minimal computational resources.

Empirical coverage analysis shows that predicted distributions remain conservative for lower-confidence intervals and near-nominal for higher-confidence intervals, supporting safe robot decision-making in HRC. Extensive ablation studies validated key design choices, including rotation representation, kernel, inducing points, and latent dimensionality, highlighting the framework’s efficiency and predictive reliability. Combined with modest inference times, these properties demonstrate that compact probabilistic models can be practical and reliable for downstream robotics tasks. In particular, the predicted distributions could be directly leveraged by motion planners to anticipate human motion, avoid collisions, and generate more responsive robot behaviors, pointing to potential real-time deployment in interactive HRC settings.

Future extensions will incorporate cross-joint dependencies, improve robustness to missing data, and expand capabilities to longer prediction horizons. Overall, this study positions GPs as a compact, interpretable, and well-calibrated foundation for probabilistic human motion forecasting, providing a practical alternative to larger, more complex deep learning models.

REFERENCES

- [1] W. Liu, X. Liang, and M. Zheng, “Task-constrained motion planning considering uncertainty-informed human motion prediction for human–robot collaborative disassembly,” *IEEE/ASME Trans. Mechatron.*, vol. 28, no. 4, pp. 2056–2063, 2023.
- [2] M. Faroni, M. Beschi, and N. Pedrocchi, “Safety-aware time-optimal motion planning with uncertain human state estimation,” *IEEE Robot. Autom. Lett. (RAL)*, vol. 7, no. 4, pp. 12 219–12 226, 2022.
- [3] T. Salzmann, M. Pavone, and M. Ryll, “Motron: Multimodal probabilistic human motion forecasting,” *Proc. IEEE Conf. Comput. Vis. Pattern Recognit. (CVPR)*, 2022.
- [4] E. Aksan, M. Kaufmann, P. Cao, and O. Hilliges, “A spatio-temporal transformer for 3d human motion prediction,” in *International Conference on 3D Vision (3DV)*. IEEE, 2021, pp. 565–574.
- [5] H. Ahn, E. V. Mascaro, and D. Lee, “Can we use diffusion probabilistic models for 3d motion prediction?” in *Proc. IEEE Int. Conf. Robot. Autom. (ICRA)*. IEEE, 2023, pp. 9837–9843.
- [6] Y. Ma, K. Zhou, F. Yu, F. W. Li, and X. Liang, “Uncertainty-aware probabilistic 3d human motion forecasting via invertible networks,” in *Proc. IEEE Int. Conf. Robot. Autom. (ICRA)*, 2025, pp. 14 307–14 314.
- [7] A. Kothari, T. Tohme, X. Zhang, and K. Youcef-Toumi, “Enhanced human-robot collaboration using constrained probabilistic human-motion prediction,” in *Proc. IEEE Int. Conf. Autom. Sci. Eng. (CASE)*. IEEE, 2025, pp. 541–547.
- [8] E. V. Bonilla, K. Chai, and C. Williams, “Multi-task gaussian process prediction,” *Advances in Neural Information Processing Systems*, vol. 20, 2007.
- [9] M. Titsias, “Variational learning of inducing variables in sparse gaussian processes,” in *Proceedings of the Twelfth International Conference on Artificial Intelligence and Statistics*, ser. Proceedings of Machine Learning Research, D. van Dyk and M. Welling, Eds., vol. 5. Hilton Clearwater Beach Resort, Clearwater Beach, Florida USA: PMLR, 16–18 Apr 2009, pp. 567–574. [Online]. Available: <https://proceedings.mlr.press/v5/titsias09a.html>
- [10] C. Ionescu, D. Papava, V. Olaru, and C. Sminchisescu, “Human3.6m: Large scale datasets and predictive methods for 3d human sensing in natural environments,” *IEEE Trans. Pattern Anal. Machine Intell.*, vol. 36, no. 7, pp. 1325–1339, July 2014.
- [11] J. Martinez, M. J. Black, and J. Romero, “On human motion prediction using recurrent neural networks,” in *Proc. IEEE Conf. Comput. Vis. Pattern Recognit. (CVPR)*, 2017, pp. 2891–2900.
- [12] Z. Lou, Q. Cui, T. Wang, Z. Song, L. Zhang, C. Cheng, H. Wang, X. Tang, H. Li, and H. Zhou, “Harmonizing stochasticity and determinism: Scene-responsive diverse human motion prediction,” in *Advances in Neural Information Processing Systems*, A. Globerson, L. Mackey, D. Belgrave, A. Fan, U. Paquet, J. Tomczak, and C. Zhang, Eds., vol. 37. Curran Associates, Inc., 2024, pp. 39 784–39 811.
- [13] Y. Yuan and K. Kitani, “Dlow: Diversifying latent flows for diverse human motion prediction,” in *Proc. European Conf. Computer Vision (ECCV)*. Springer, 2020, pp. 346–364.
- [14] S. Tian, M. Zheng, and X. Liang, “Transfusion: A practical and effective transformer-based diffusion model for 3d human motion prediction,” *IEEE Robot. Autom. Lett. (RAL)*, vol. 9, no. 7, pp. 6232–6239, 2024.
- [15] J. Xu, X. Chen, X. Lan, and N. Zheng, “Probabilistic human motion prediction via a bayesian neural network,” in *Proc. IEEE Int. Conf. Robot. Autom. (ICRA)*. IEEE, 2021, pp. 3190–3196.
- [16] J. M. Wang, D. J. Fleet, and A. Hertzmann, “Gaussian process dynamical models for human motion,” *IEEE Trans. Pattern Anal. Machine Intell.*, vol. 30, no. 2, pp. 283–298, 2008.
- [17] A. Damianou, M. Titsias, and N. Lawrence, “Variational gaussian process dynamical systems,” *Advances in Neural Information Processing Systems*, vol. 24, 2011.
- [18] J. Zhao and S. Sun, “Variational dependent multi-output gaussian process dynamical systems,” *Journal of Machine Learning Research*, vol. 17, no. 121, pp. 1–36, 2016. [Online]. Available: <http://jmlr.org/papers/v17/14-423.html>
- [19] W. Guo, Y. Du, X. Shen, V. Lepetit, X. Alameda-Pineda, and F. Moreno-Noguer, “Back to mlp: A simple baseline for human motion prediction,” in *Proc. IEEE Winter Conf. on Applications of Computer Vision (WACV)*, 2023, pp. 4809–4819.
- [20] L.-H. Chen, J. Zhang, Y. Li, Y. Pang, X. Xia, and T. Liu, “Humanmac: Masked motion completion for human motion prediction,” in *Proc. IEEE Int. Conf. Comput. Vis. (ICCV)*, 2023, pp. 9544–9555.
- [21] D. Pavllo, C. Feichtenhofer, M. Auli, and D. Grangier, “Modeling human motion with quaternion-based neural networks,” *International Journal of Computer Vision*, vol. 128, no. 4, pp. 855–872, 2020.
- [22] D. Wei, H. Sun, B. Li, J. Lu, W. Li, X. Sun, and S. Hu, “Human joint kinematics diffusion-refinement for stochastic motion prediction,” in *Proceedings of the AAAI Conference on Artificial Intelligence*, vol. 37, no. 5, 2023, pp. 6110–6118.
- [23] Y. Zhou, C. Barnes, J. Lu, J. Yang, and H. Li, “On the continuity of rotation representations in neural networks,” in *Proc. IEEE Conf. Comput. Vis. Pattern Recognit. (CVPR)*, 2019, pp. 5745–5753.
- [24] W. Mao, M. Liu, and M. Salzmann, “History repeats itself: Human motion prediction via motion attention,” in *Proc. European Conf. Computer Vision (ECCV)*. Springer, 2020, pp. 474–489.
- [25] Y. Yuan and K. Kitani, “Diverse trajectory forecasting with determinantal point processes,” *Int. Conf. on Learning Representations*, 2020.
- [26] X. Yan, A. Rastogi, R. Villegas, K. Sunkavalli, E. Shechtman, S. Hadap, E. Yumer, and H. Lee, “Mt-vae: Learning motion transformations to generate multimodal human dynamics,” in *Proc. European Conf. Computer Vision (ECCV)*, 2018, pp. 276–293.